Do Interictal Epileptiform Discharges and Brain Responses to Electrical Stimulation Come from the Same Location? An Advanced Source Localization Solution

Sepehr Shirani, Bahman Abdi-Sargezeh, Antonio Valentin, Gonzalo Alarcon, Jordan Bird, and Saeid Sanei, Senior Member, IEEE

***Abstract*—Identification of seizure sources in the brain is of paramount importance, particularly for drug-resistant epilepsy patients who may require surgical operation. Interictal epileptiform discharges (IEDs), which may or may not be frequent, are known to originate from seizure networks. Delayed responses (DRs) to brain electrical stimulation have been recently discovered. If DRs and IEDs come from the same location and the DRs can be accurately localized, there will be a significant step in identification of the seizure sources. The solution to this important question has been investigated in this paper. For this, we have exploited the morphology of these spike-type events, as well as the variability in their temporal locations, to develop new constraints for an adaptive Bayesian beamformer that outperforms the conventional and recently proposed beamformers even for identifying correlated sources. This beamformer is applied to an array (a.k.a mat) of cortical EEG electrodes. The developed approach has been tested on 300 data segments from five epileptic patients included in this study, which clinically represent a large population of candidates for surgical treatment. As the significant outcome of applying this beamformer, it is very likely (if not certain) that for an epileptic subject, the IEDs and DRs originate from the same location in the brain. This paves the way for a quick identification of the source(s) of seizure in the brain.**

***Index Terms*—Adaptive beamformer, delayed response, EEG, epilepsy, IED, multiple constraints, seizure, SPES.**

I. Introduction

THE benefit of interictal electroencephalogram (iEEG) recordings for investigation of interictal epileptiform discharges (IEDs) for presurgical assessment, especially for drug-resistant epilepsy (DRE) cases, has long been investigated [1]. Early studies have shown several patterns of IEDs at the source of seizure and other regions, some located in the opposite hemisphere [2], [3] pointing out their limited localizing power due to the lack of clear criteria to identify those associated with the epileptogenic zones [4]. Moreover, the IEDs may not be frequently visible in iEEGs. Single pulse electrical stimulation (SPES) has been established as a practical tool to identify the epileptogenic zone during interictal periods [5]–[8]. Previous research has shown that the responses to SPES can be categorized into two groups: early responses (ERs) and delayed responses (DRs) [9]. ERs are observable locally or over regions connected to the stimulated cortex when stimulating most cortical areas. They usually consist of a sharp deflection instantly after the stimulus artifact, sometimes

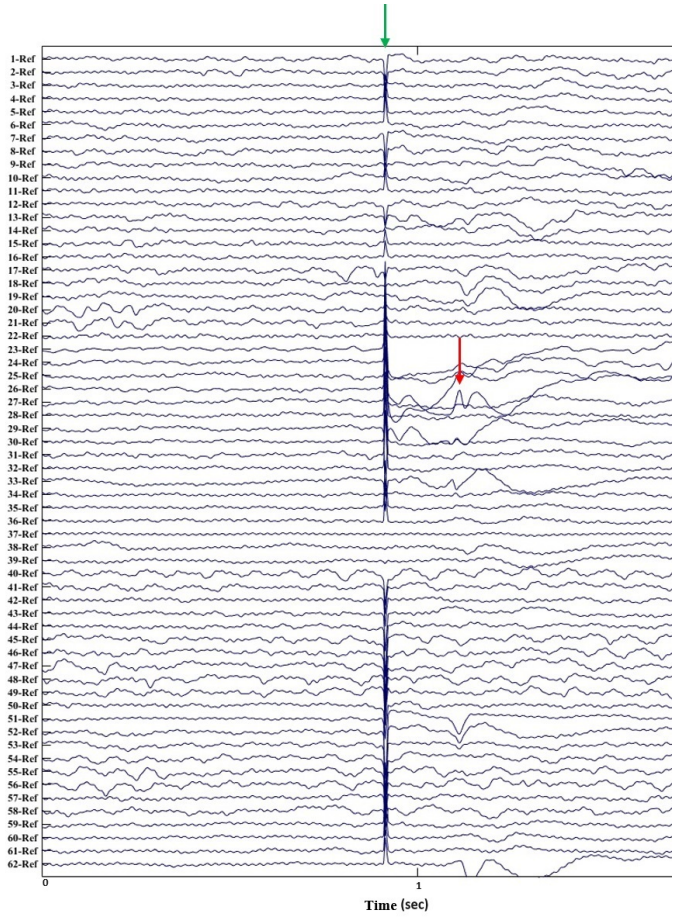

Fig. 1: Recorded data using the intracranial electrodes. This figure shows a selected segment of SPES recordings with stimulation artifacts indicated with the green arrow and the DRs visible in the data with the red arrow.

S. Shirani and J. Bird are with the Department of Computer Science, Nottingham Trent University, Nottingham, United Kingdom.

B. Abdi-Sargezeh is with the Department of Clinical Neurosciences, University of Oxford, Oxford, United Kingdom.

A. Valentin is with the Department of Basic and Clinical Neuroscience, King's College London, London, United Kingdom.

G. Alarcon is with the Department of Clinical Neurophysiology, University of Manchester, Manchester, United Kingdom.

S. Sanei is with the Department of Electrical and Electronic Engineering, Imperial College London, London, United Kingdom.

This article has been accepted for publication in IEEE Transactions on Biomedical Engineering. This is the author's version which has not been fully edited and content may change prior to final publication. Citation information: DOI 10.1109/TBME.2024.3392603

blended with it, followed by a slow wave with their amplitude depending on the stimulation intensity, and are considered normal cortical responses to SPES. In contrast to ERs, DRs (with latency greater than 100 ms and up to 1 second) are considered to be associated with seizure network. Previous clinical research on SPES has shown that if there is a specific functional connectivity between the location of the stimulation and the hyperexcitable region responsible for seizure, the DRs can be observable in the hyperexcitable region [5]–[7], [9], [10]. It has been shown that a DR consists of one or multiple spikes followed by a slow wave and generally resembles the IEDs [11]–[13]. This resemblance can be used as an interictal marker for the seizure source. However, there are some reports showing that in a considerable number of cases (approximately 20% to 30%), the highest amplitude and incidence for IEDs are in regions other than seizure onset [11]. We stress that the IEDs may not be frequent and IEDs or DRs may not be visible in the iEEG if the electrodes are not implanted near their generators. Therefore, it is crucial to identify the IED and DR sources using a suitable and accurate localization algorithm and check if they always come from the same location in the brain. If this happens to be true, it is not necessary to wait for IED elicitation and bear the ambiguity in identification while it is possible to identify the DRs by brain stimulation. To identify the source of IEDs and DRs, the overlap between them, and their association with seizure onset and seizure network in general, a robust source localization pipeline is needed. Often, it is difficult to implant the iEEG electrodes close enough to the seizure source.

Beamforming, a concept in array processing, is an established method for localizing sources from multichannel EEG or magnetoencephalogram (MEG) [14]. It involves tracking the signal source whose influence is distributed over an array of sensors [15].

A popular beamforming method is linearly constrained minimum variance (LCMV) beamforming [14], [16], [17]. The conventional LCMV beamformer, as a generalized minimum distortionless response (MVDR) beamformer, minimizes the output power while preserving a constant response in the direction of activity of interest. Despite its popularity, the LCMV beamformer is not robust when the signal-to-noise ratio (SNR) is low or in the case of multiple possibly correlated sources [18]. A common approach to solve this problem is to average over a large number of segments in which the variability of the source activity is ignored and therefore, the sensitivity and accuracy of the localization methods are reduced. DRs and IEDs as spike-like transients demonstrate some differences in morphology, power, and latency for intra-subject trials, and therefore, employment of conventional beamforming methods combined with averaging technique over various epochs can lead to misleading results. To solve this problem in a recent work, a novel adaptive iterative LCMV beamformer (AI-LCMV) was developed and employed to identify the DR sources where the use of a template as the desired source in the form of an additional constraint improved the localization accuracy and to a degree solved the conventional LCMV beamformer sensitivity to low SNR activity [19].

Although the AI-LCMV beamformer demonstrated a significant improvement over the conventional method, especially when the DRs are not visible to the implanted electrodes, due to the temporal mismatch between the template and the DRs the performance is still questionable. This is due to using Euclidean distance as the similarity measure. Another limitation of the AI-LCMV beamformer, similar to the conventional method, is its low sensitivity to multiple nearby sources

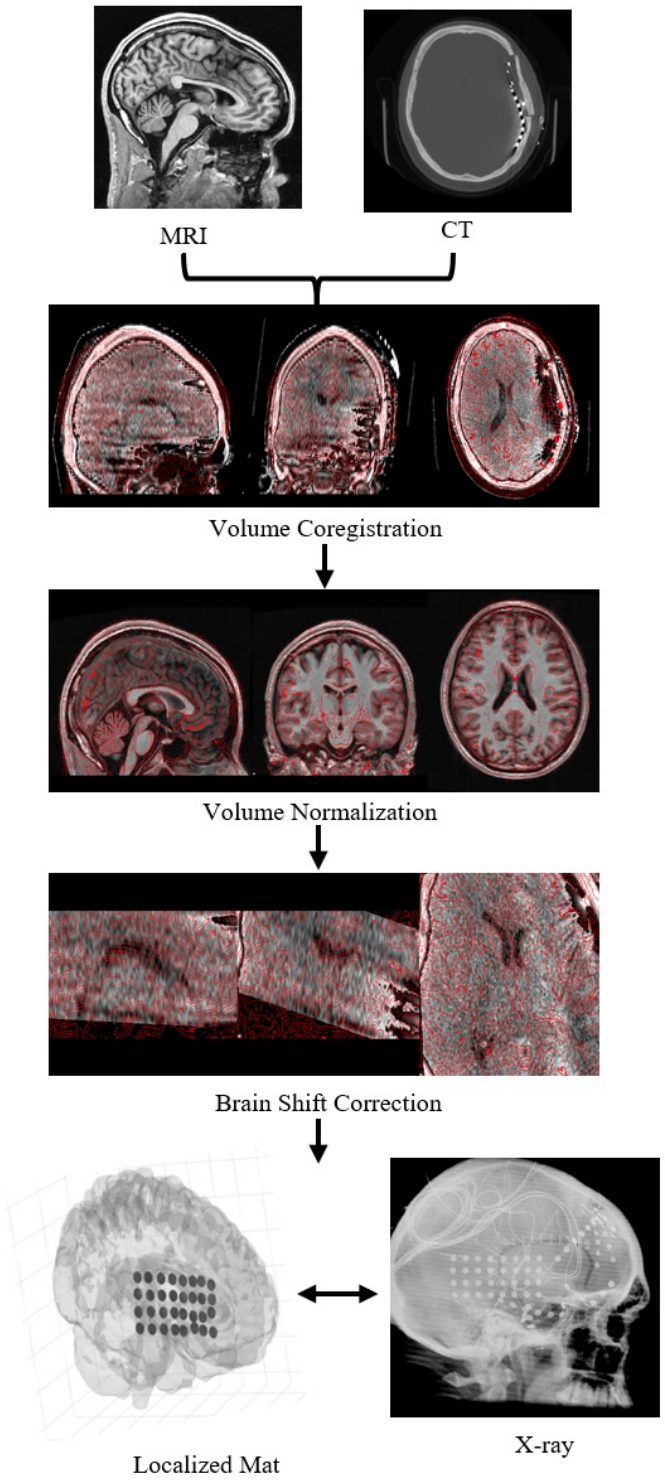

Fig. 2: Pipeline for coregisteration of pre- and post-surgery CT and MRI images and localization of intracranial electrodes.

which may be temporally or spatially correlated. To mitigate the effect of correlated sources, a model data covariance estimation by sparse Bayesian learning (SBL-BF) has recently been incorporated into the localization formulation [20]. As a result, the performance compared to conventional LCMV beamformer of identifying multiple correlated sources has been improved [20].

Here, a new adaptive beamforming pipeline named adaptive Bayseian beamformer with multiple constraints (ABMC) employs the cross-correlation between the selected template and the beamformer output as the additional constraint to the minimum variance beamformer. Then, it incorporates sparse Bayesian learning for covariance estimation in which any possible correlation between active sources is exploited and canceled out. In the cases where DRs or IEDs are temporally or spatially close to each other (or correlated), this approach improves their localization. The ABMC beamformer developed here not only considers the morphology of IEDs and DRs as the desired source but also mitigates the effects of correlated sources using the covariance of input signals.

II. Data

The EEG [21] signals recorded and used for this study have been collected from five subjects included in this study using the implanted intracranial electrodes following the standard clinical assessment procedure employed at King's College London Hospital. For each subject, the unique SPES setup, including the type, number, and locations of the electrodes, are chosen considering the presumed location of epileptogenic regions. The criteria for selection and implantation process for DRE patients have been described in [22]. The data for SPES sessions and interictal periods have been recorded using the system and methods described previously [23]. The interictal data are recorded during both sleep and awake periods. The SPES is performed using a pair of electrodes via an authorized constant current of 1-8mA, frequency of 0.2 Hz, at a duration of 1ms, employing a neurotransmitter while the signals are recorded by the remaining electrodes that are not used for stimulation. All subjects included in this study have a subdural mat placed over the cortex, each with 20 or 32 platinum contacts with 10mm center-to-center intervals, used as the input sensor array to the proposed beamformer (excluding the pair of electrodes used for stimulation). The recording setup and SPES parameters are chosen based on gold-standard medically approved practice to avoid tissue damage or any other problem for the subjects, and we had no control over these parameters.

Figure 1 illustrates a sample window selected from the SPES recordings that contains examples of visible DRs. Table I shows the information for each case, including the number and location of the intracranial electrodes and the surgical operation outcome based on the Engel Outcome Scale (EOS) [24]. Here, pre-surgery magnetic resonance imaging (MRI) and post-surgery computed tomography (CT) scans are used to localize the positions of the implanted electrodes and measure the head model and leadfield matrix as the linear operator that links the brain activity sources to the recording signals. The coregistration of pre-operation MRI and post-operation CT is done in a pipeline implemented in Lead-DBS [25], in which the CT images are first registered to MRIs, then the volumes are normalized, and finally, the possible brain shift due to the surgery is compensated [26]–[28]. The coregistration results are used to localize the electrodes using Fieldtrip [29] and LeGUI [30] separately and then compared by experts to make sure the localization results are as accurate as possible. Finally, the co-registered images and electrode positions are used to measure the leadfield matrix for the beamformer. As various pairs of electrodes are used for stimulation during the SPES session for each case, the leadfield matrix is measured multiple times for each subject if necessary. Figure 2 shows the pipeline for coregistration of pre- and post-operation images.

TABLE I: The number and locations of implanted electrodes alongside the result of surgery for each case (R=Right, L=Left, T=Temporal, F=Frontal, A=Anterior, P=Posterior, O=Occipital, In=Insular, H=Hippocampus, M=Mesial).

Case	Number and electrodes locations	EOS
1	20 LT, 4 Posterior Superior Parietal, 8 Mid Parietal, 8 Inferior Parietal	No surgery
2	32 RT, 8 RF, 8 Central	II
3	20 RT, 8 RF, 8 AT, 8 SubT	No surgery
4	32 RT, 5 Tpole, 5 MT, 5PMT, 5 AIn, 5 MIn, 5 PIn	I
5	32 RT, 8 RATP, 8 RAT, 8 RMT, 8 RPT	II

III. Method

The conventional LCMV beamformer attempts to localize the source by maximizing the received power [14], [16], [17]. Due to the sensitivity of the LCMV beamformer to the power of the obtained signal, it is not the ideal approach when encountering low-power spike-like activities such as DRs and IEDs. Another disadvantage of the LCMV beamformer is its disability to distinguish nearby highly correlated sources. When signals from various sources are highly correlated or closely spaced, the spatial filter may not effectively distinguish between them. This can result in spatial aliasing, where the beamformer cannot determine the individual sources and treats them as a single source. Here, the ABMC beamformer is developed such that by employing a sparse Bayesian algorithm for covariance estimation, the possible effect of correlated sources is excluded, and the cross-correlation between the beamformer output and the desired template is used as an additional constraint. The DRs and IEDs templates as the desired source for each subject are selected from the annotated visible waveforms compatible with the overall morphology of DRs and IEDs from the same subject (often the channel closest to the hyperexcitable region responsible for seizure). This is to compensate for any possible delay mismatch between the beamformer's output and the selected template as the desired source. The DR and IED templates as the desired source for each subject are selected from the annotated visible waveforms compatible with the overall morphology of DRs and IEDs from the same subject (often the channel closest to the hyperexcitable region responsible for seizure).

Here, in each iteration, the algorithm adjusts the weighting coefficients to minimize the output signal variance, similar to

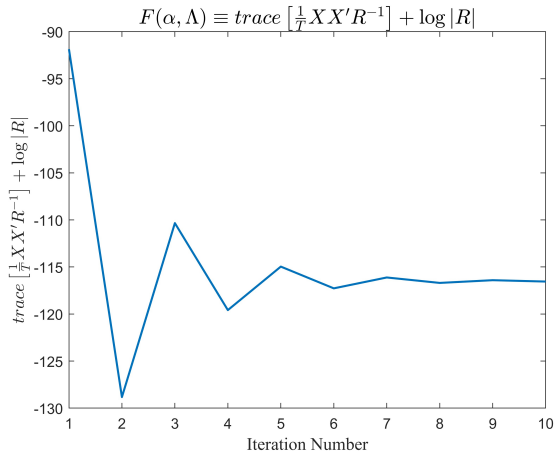

Fig. 3: Convergence plot for $\left(\text{trace}\left[\frac{1}{T}XX^{\intercal}R^{-1}\right] + \log|R|\right)$ after 10 iterations for a selected segment of data.

the primary objective of the conventional LCMV beamformer while adhering to an additional constraint. This constraint exploits the maximum cross-correlation between the output of the beamformer and the template for the desired source at the correct time lag. After sufficient iterations, the ABMC algorithm converges to the optimal weighting coefficient of the beamformer. The formulations for the ABMC beamformer are presented below.

Consider the brain source activity $s\left(t\right) = \left[s_1\left(t\right),\ldots,s_N\left(t\right)\right]^{\intercal}$ at time point t (t=1,…,T), and the leadfield matrix $G = \left[g_1 \ldots g_N\right] \epsilon \mathbb{R}^{M\times N}$ where M is the number of electrodes in the subdural mat (i.e. recorded signals) and N is the number of grid points in the head model. Then, the linear model for brain activity can be presented as:

$$x\left(t\right) = \sum_{n=1}^{N} s_n(t) g_n + \varepsilon(t) \tag{1}$$

where $x\left(t\right) = \left[x_1(t),\ldots,x_M\left(t\right)\right]^{\intercal}$ is the recorded signal using a subdural mat and $\varepsilon(t)$ represents the noise. This equation is initially presented for scalar values, but an extension to vector leadfields that considers source orientation in three-dimensional head model is utilized in the calculations. Additionally, for simplicity we define $X = [x(1), ..., x(T)]$, and $S = [s(1), ..., s(T)]$.

To estimate the input signal array covariance via sparse Bayesian learning, Equation (1) is converted into its probabilistic form. This conversion involves defining prior distributions for the unknown variables, outlined as follows:

$$\left(x\left(t\right) \mid s\left(t\right)\right) = N(x(t)|Gs\left(t\right), \Lambda) \tag{2}$$

Here, the diagonal noise covariance is denoted as Λ= diag($\lambda_1,\ldots,\lambda_M$). The noise is assumed to have a zero-mean Gaussian distribution. The source prior distribution is represented as:

$$p\left(s\left(t\right) \mid \alpha\right) = \prod_{n=1}^{N} N(s_n(t)|0, \alpha_n) \tag{3}$$

where $\alpha = diag(\alpha_1, \ldots, \alpha_N)$ and α_n is the prior variance for the activity of the n-th grid location in the head model. The process of estimating hyperparameters and noise covariance for each voxel is linked to the maximization of the marginal likelihood $p\left(X \mid \alpha, \Lambda\right)$.

$$p\left(X \mid \alpha, \Lambda\right) = \prod_{t=1}^{T} N(x(t)|0, R) \tag{4}$$

The input signal covariance R can be expressed as a matrix in which the sources are assumed to be uncorrelated, and α is considered as an uncorrelated source covariance matrix, where

$$R = G\alpha G^{\intercal} + \Lambda \tag{5}$$

The estimation of hyperparameters and data covariance can be achieved through type-II maximum likelihood or by minimizing the cost function [20]:

$$\begin{aligned} F(\alpha,\Lambda) &\triangleq -2\log p\left(X \mid \alpha,\Lambda\right) \\ &\equiv \text{tr}\left[\frac{1}{T}XX^{\intercal}R^{-1}\right] + \log|R| \end{aligned} \tag{6}$$

To minimize the non-convex cost function in (6), a majorization-minimization approach [31] is followed, providing a convex upper-bound limit as an alternative cost function for optimization of each grid point. Here, $z = diag(z_1, \ldots, z_N)$ and $h = diag(h_1, \ldots, h_M)$ are auxiliary parameters, with z_0 and h_0 being scalar terms dependent only on z and h [32], [33].

$$\begin{aligned} F\left(\alpha\right) =& \frac{1}{T}\sum_{t=1}^{T} x^{\intercal}(t)R^{-1}x(t) + \log|R| \\ \leq& \frac{1}{T}\sum_{t=1}^{T}\left[\left(x(t) - G\overline{S}(t)\right)^{\intercal}\Lambda^{-1}\left(x(t) - G\overline{S}(t)\right)\right] \\ &+ \frac{1}{T}\sum_{t=1}^{T}\left[\overline{s}^{\intercal}(t)\alpha^{-1}\overline{s}(t)\right] + \text{tr}\left(z^{\intercal}\alpha\right) - z_0 \end{aligned} \tag{7}$$

$$\begin{aligned} F\left(\Lambda\right) =& \frac{1}{T}\sum_{t=1}^{T} x^{\intercal}(t)R^{-1}x(t) + \log|R| \\ \leq& \frac{1}{T}\sum_{t=1}^{T}\left[\left(x(t) - G\overline{S}(t)\right)^{\intercal}\Lambda^{-1}\left(x(t) - G\overline{S}(t)\right)\right] \\ &+ \frac{1}{T}\sum_{t=1}^{T}\left[\overline{s}^{\intercal}(t)\alpha^{-1}\overline{s}(t)\right] + \text{tr}\left(g^{\intercal}\Lambda\right) - g_0 \end{aligned} \tag{8}$$

The convex bounding update rule for the n-th grid position variance and m-th channel noise variance is derived by equalling the derivatives of $F(\alpha)$ and $F(\Lambda)$ with respect to α_n and λ_m to zero, resulting in:

$$\widehat{\alpha}_n = \sqrt{\frac{\frac{1}{T}\sum_{t=1}^{T}\overline{s}_n^2}{\hat{z}_n}} \tag{9}$$

$$\widehat{\lambda}_m = \sqrt{\frac{\left[\sum_{t=1}^{T}\left(x\left(t\right) - G\overline{s}(t)\right)\left(x\left(t\right) - G\overline{s}(t)\right)^{\intercal}\right]_{mm}}{T\hat{h}_m}} \tag{10}$$

The update rule for z and h involves finding two hyperplanes $z^{\intercal}\alpha - z_0$ and $h^{\intercal}\Lambda - h_0$ that tightly bound R given α and

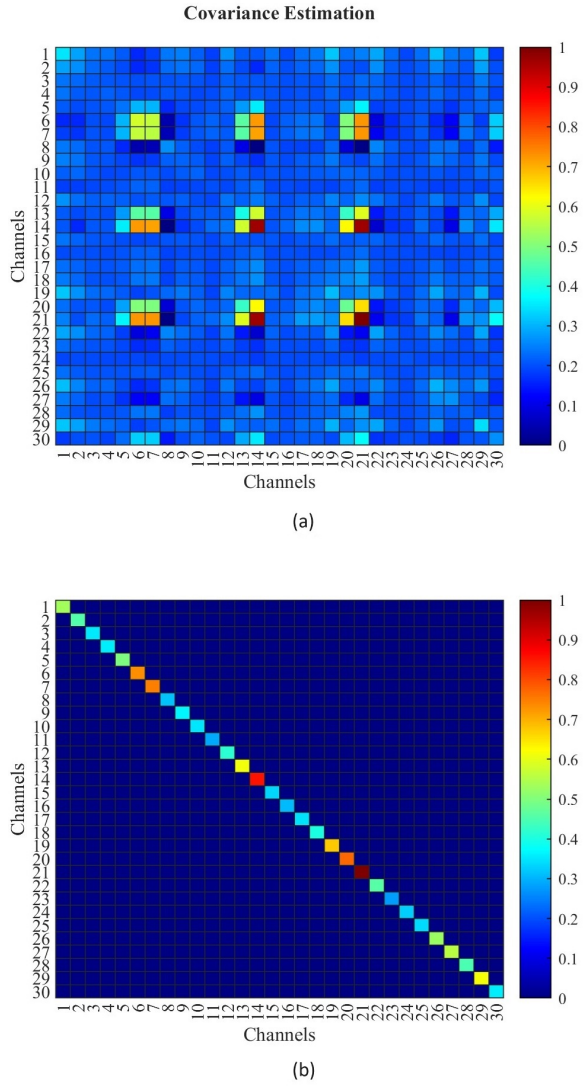

Fig. 4: The covariance of (a) input signal X (i.e. $\frac{1}{T}XX^{\intercal}$) and (b) the estimated covariance using sparse Bayesian learning algorithm after sufficient iterations.

Λ. These hyperplanes, tangential to R [34], lead to updated values for z and g given by:

$$\hat{z}_n = g_n^{\intercal} R g_n \tag{11}$$

$$\hat{g}_m = (R)_{mm} \tag{12}$$

The update rule for $\overline{s}_n(t)$ is presented in:

$$\overline{s}_n(t) = \widehat{\alpha}_n g_n^{\intercal} R x(t) \tag{13}$$

The iterative estimation process for the covariance of the input signals, while excluding the effect of correlated sources, involves iterating across equations (9) to (13) and substituting α and Λ in equation (5). Figure 3 illustrates the convergence plot for equation (6) after ten iterations. After sufficient iterations, the estimated covariance is then adaptively used to estimate the weights for the beamformer. Figure 4 shows the estimated covaraince for a segment of data.

Considering the aim of the ABMC beamformer to minimize the output power while matching the output to the desired source, the weight vector W for each of the x, y, and z directions in the three-dimensional space is the solution to the following multiple linearly constrained optimization problem:

$$\underset{W}{\text{Min}} \left(\frac{1}{2} W^{\intercal} R W \right)$$
$$\text{subject to} \quad G^{\intercal} W = f \quad \& \quad \underset{W}{\text{Max}} \; (W^{\intercal} X \cdot u)$$

where R is the estimated covariance matrix, W is the weight vector for the beamformer, and u (a visible IED or DR template selected from the recordings) in the additional constraint refers to the desired template with the same length as X. Figure 5 shows an example of different IEDs observed in the data for one subject. This optimization problem can be executed iteratively after converting the constrained problem to an unconstrained format using Lagrange multipliers:

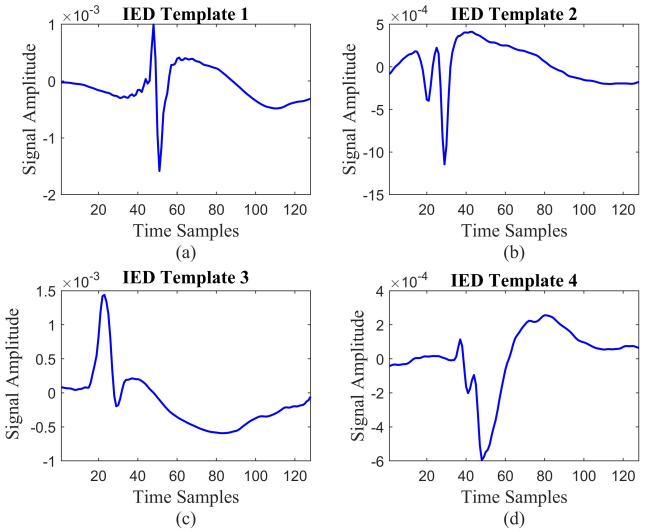

Fig. 5: Various templates used as the desired source for identification of the IED source for one subject.

$$J(W) = Min(\frac{1}{2} W^{\intercal} R W + \beta_1 (f - G^{\intercal} W) + \beta_2 (W^{\intercal} X \cdot u)) \tag{14}$$

where β_1 and β_2 are the penalty terms or Lagrange multipliers. By measuring the gradient with respect to W the following equation can be reached:

$$W(n+1) = W(n) - \mu \nabla_W J(W(n)) \tag{15}$$

where

$$\nabla_W J(W(n)) = RW(n) - \beta_1 G - \beta_2 X u^{\intercal} \tag{16}$$

with $u^{\intercal}$ at lag j ($u^{\intercal}(m+j)$). The following iterative process is used to estimate W:

$$W(n+1) = W(n) - \mu (RW(n) - \beta_1 G - \beta_2 X u^{\intercal}) \tag{17}$$

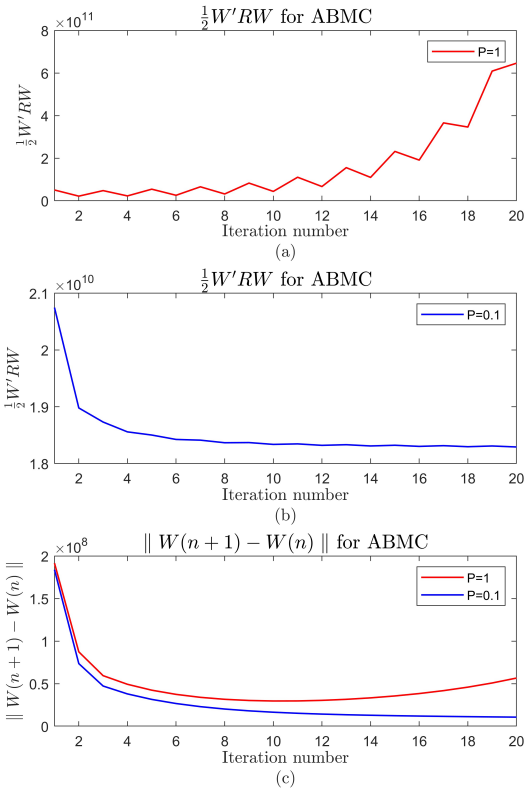

Fig. 6: The convergence plot for $\frac{1}{2}W^{\intercal}RW$ and $\| W(n+1) - W(n) \|$ for different P values over 20 iterations.

where μ is the non-negative step size for each iteration. Considering the constraint $G^{\intercal}W = f$, pre-multiplying both sides of (17) by $G^{\intercal}$ yields:

$$f = G^{\intercal}W(n) - \mu(G^{\intercal}RW(n) - \beta_1 G^{\intercal}G - \beta_2 G^{\intercal}Xu^{\intercal}) \quad (18)$$

By considering β_2 as β_2 = Pβ_1, β_1 can be obtained from (18) as:

$$\beta_1(n) = \frac{f - G^{\intercal}W(n) + \mu G^{\intercal}RW(n)}{\mu G^{\intercal}G + \mu \mathrm{P} G^{\intercal}Xu^{\intercal}} \quad (19)$$

By replacing the values for β_1 and β_2 in (17) $W(n+1)$ is calculated in each iteration. The initial W is set to an $M \times 1$ vector of zero values. The value of step size μ and the ratio between β_1 and β_2 (P) are empirically adjusted according to the convergence rate for $\frac{1}{2}W^{\intercal}RW$ and $\| W(n+1) - W(n) \|$. If P is too low, the weight for the second constraint related to the desired template for the ABMC becomes negligible, and the output becomes similar to those of conventional iterative LCMV beamformer. Also, increasing the value of P up to a specific threshold for each segment causes $\frac{1}{2}W^{\intercal}RW$ and $\| W(n+1) - W(n) \|$ not to converge, and therefore, the optimal value for the ABMC beamformer weight cannot be reached. Figure 6 shows the values of $\frac{1}{2}W^{\intercal}RW$ and $\| W(n+1) - W(n) \|$ for a selected segment over 20 iterations.

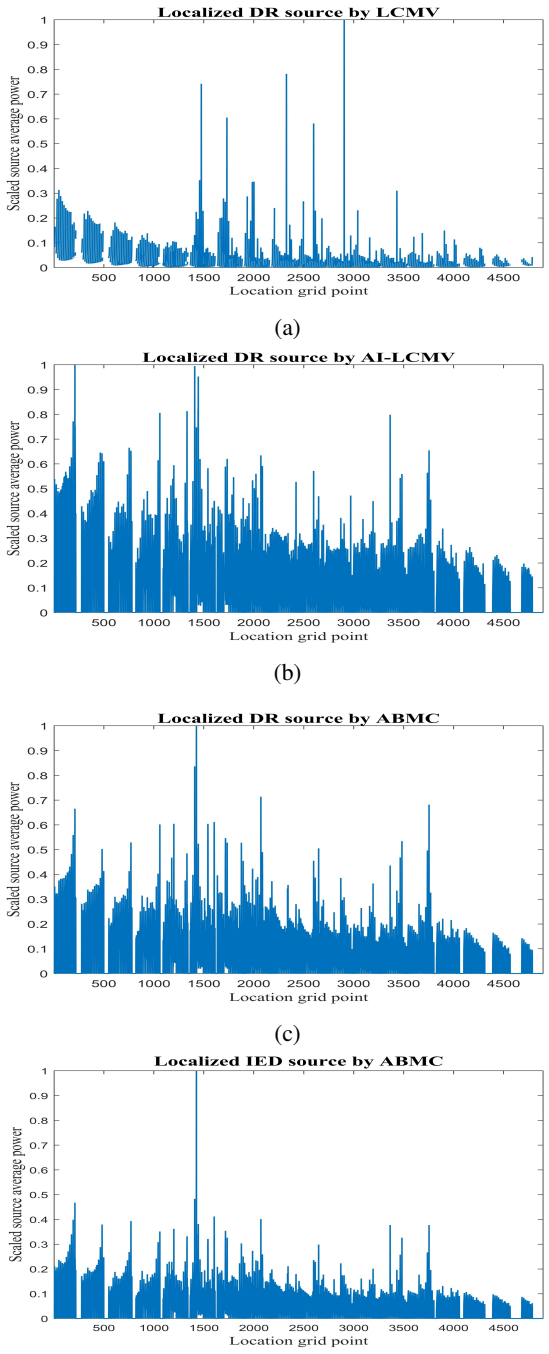

Fig. 7: Localized DRs to the SPES from a sample segment using (a) conventional LCMV, (b) AI-LCMV, and (c) ABMC approaches for one subject. Plot (d) indicates the localized IEDs using the ABMC approach for the same case. As shown in this figure, conventional LCMV approach identifies a different region as the source compared to that by the adaptive methods. The ABMC demonstrates the highest accuracy and consistency in localization. Most importantly, ABMC localizes the DRs and IEDs of a subject at the same position in the brain.

IV. Results

Throughout the following experiments, we first try to demonstrate the performance of ABMC and second verify that

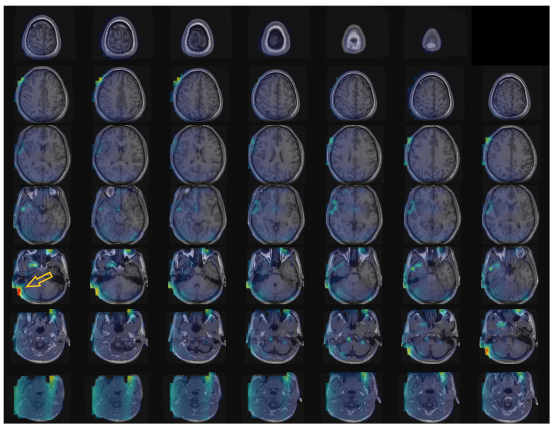

(a) Localized DR source

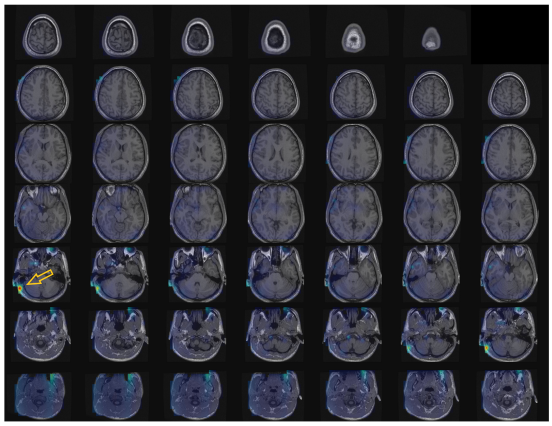

(b) Localized IED source

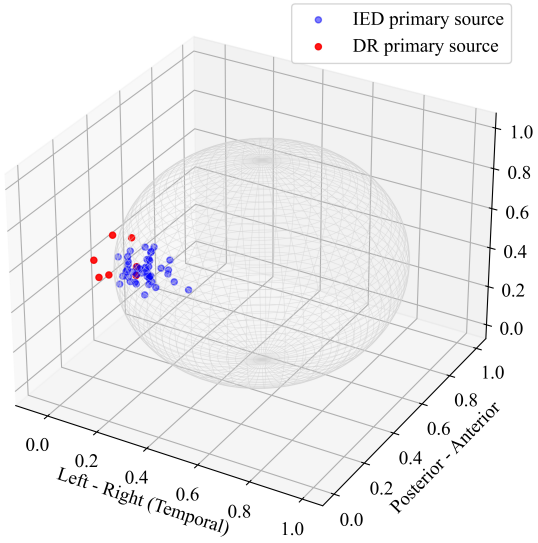

(c) Localized IEDs and DRs for tested segments

Fig. 8: The identified sources (pointed to with yellow arrow) for (a) DRs and (b) IEDs using the ABMC beamformer for a subject with a clinical report of clear regional abnormal responses to SPES, in the posterior and lateral aspect of the left temporal lobe suggesting that this region is hyperexcitable and potentially epileptogenic. Plot (c) shows the normalized locations of IED (blue) and DR (red) sources for various iEEG segments.

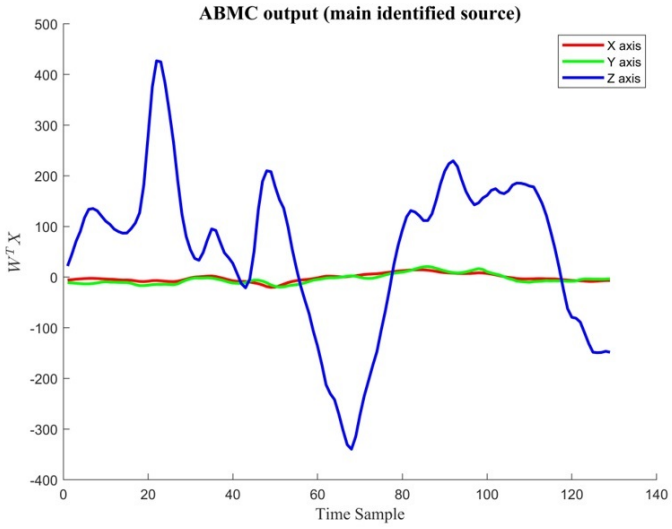

(a)

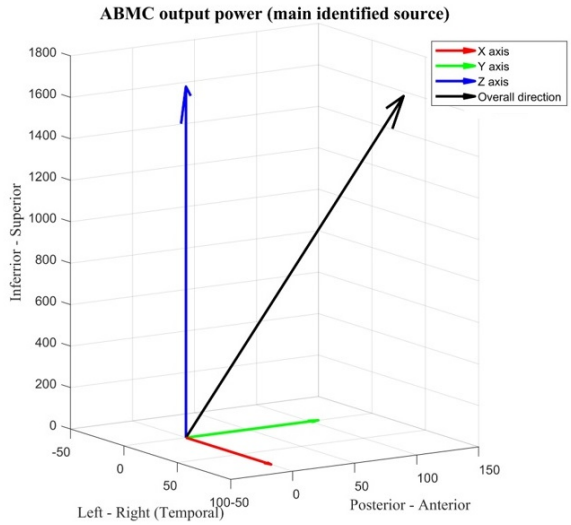

(b)

Fig. 9: (a) The output of ABMC beamformer for the grid point identified as the main source along each axis and (b) the overall direction of source activity based on the received power along each axis.

IEDs and DRs originate from the same location in the brain of each of the subjects. The ABMC beamformer developed in this study has been used for 300 data segments, each 0.5 seconds long. These include 93 segments with visible DRs and 57 segments from the same SPES sessions where the DRs were not visible to the implanted electrodes. Initially, the segments containing DRs were fed to the ABMC and AI-LCMV beamformers. The general results for the subjects included in this study indicated that, although the identified sources using both approaches were close to the lead electrode

at the seizure source (hyperexcitable region), the identified source using the ABMC beamformer was, on average, 0.82 cm closer to the seizure onset and, also, more consistent compared to those achieved by AI-LCMV for the tested segments with visible DRs. Similarly to the segments with visible DRs, in the tested segments where no DRs were visible to the implanted electrodes, the identified primary source using the ABMC approach was, on average, 1.35 cm closer to the hyperexcitable region compared to those achieved by the AI-LCMV method. The detailed results for each case are reported in Table II. Figure 7 shows the localized source for a selected segment of visible DRs using conventional LCMV, AI-LCMV, and ABMC approaches.

In addition to DRs, for each case, 145 segments of data with visible IEDs are fed to the ABMC beamformer for source localization. For each case, multiple IED templates observed and annotated by the experts have been used as the desired template for the beamformer. Using the ABMC beamformer, the localized sources for these segments were compared to the primary identified source for DRs selected from the SPES sessions and lead electrode at seizure onset (hyperexcitable region). The source localization results for IEDs show similar regions to those achieved from DRs, with a slightly higher average distance between the primary source and the seizure onset in general. The details related to the average distance between the identified source for each specific IED template and the lead channel at seizure source, alongside the similarity of the selected template with that of DRs for the same subject, are presented in Table III. The similarity in morpholgy of the selected templates is measured using the adaptive signed correlation index [35]. Figure 8 compares the locations identified as the primary source of DRs and IEDs for one subject. Figure 9 shows the output of ABMC algorithm for the main identified source along each axis in the three-dimensional space with the overall orientation of activity. The results from the selected segments indicated that overall, for 90% of the segments, the sources responsible for DRs and IEDs are in the same hemisphere and in proximity to the lead electrode at seizure onset. However, for 10% of the segments, including DRs or IEDs, the source was in the opposite hemisphere, far from the origin of DRs and seizure source. This is very likely to be an estimation error due to the existence of spurious sources and head model estimation. Although there might be room for improving the beamforming algorithm, the head model and leadfield matrix estimation errors play a crucial role here. This is because the ABMC identified these locations after recalculating the head model and leadfield matrix considering the changes in the SPES setup. This shows that this is most likely related to the error in leadfield and head model estimation not the selected template as the desired source or the beamformer's overall algorithm.

V. Discussion

A robust method to identify the hyperexcitable and epileptogenic regions responsible for generating DRs and IEDs can help maximize the efficiency of the clinical assessment procedure, such as SPES recordings for DRE patients. It can also be used to verify that DRs and IEDs come from the same location in the brain. Considering that for a large number of cases, regions such as the amygdala, hippocampus, frontal cortex, temporal cortex, and olfactory cortex are frequently noted as potentially epileptogenic [36], a reliable beamforming approach can help identify activity such as DRs even when the source responsible for these waveforms is not close and therefore visible to the implanted electrodes.

Although previous research has shown the benefit of applying conventional beamforming approaches like LCMV in seizure localization [37], identifying the regions responsible for generating low power, spike-like activity such as DRs, which are not necessarily consistent in morphology, is problematic. This is because these methods are sensitive to input signal power and have a high error in identifying highly correlated activities. Here, the ABMC beamformer is developed to identify the regions responsible for the DRs and IEDs, considering the similar morphology between these activities, and most importantly, verify that for a subject these two originate from the same seizure generator [11].

The advantage of proposed ABMC method compared to the conventional methods becomes more evident when the power of DRs and IEDs is low. This advantge is clear when comparing the results of the developed approach here with those achieved using conventional methods [19]. Compared to the previously established AI-LCMV, ABMC approach the results were more accurate (considering the distance between the identified primary source and the epileptogenic region confirmed using the available implanted electrodes) and more consistent across the tested segments. The ABMC beamformer employed here not only alleviates the sensitivity to the power of the recorded signals, but also can exploit the sparsity and temporal location variation of the DRs and IEDs. Although the iterative process can be time-consuming and computationally expensive, the clinical benefits of this robust localization method are invaluable. Considering the results of recent research indicating the capability of high-density EEG setups compared to stereo EEG [38], the ABMC beamformer developed here can significantly contribute to the non-invasive localization of seizure generators within the epileptic brain. Here, the DRs and IEDs selected for the templates as the desired source for each subject are often selected from the lead channel at seizure start, and the algorithm relies on the cross-correlation measurement in the second constraint to compensate for the possible delayed mismatch between the output and the desired template. One possible area to improve the beamforming algorithm is to use a time-distributed approach by developing a cooperative beamformer alongside a more comprehensive dictionary of desired templates for DRs and IEDs, which might help exploit better and adapt to temporal variations, which leads to improved reliability and performance considering the dynamic nature of DRs.

Having mentioned the benefits of the proposed ABMC method, it is important to note that, although the head model and leadfield vectors are measured multiple times according to the SPES setup for each case using the available software, improving the electrode localization and head model estimation can significantly improve the accuracy and reliability of

TABLE II: The number of tested segments for each case where DRs were visible and invisible after stimulation alongside the distance (Euclidean) between the localized and actual sources using AI-LCMV and ABMC methods (N: number of tested segments).

	AI-LCMV				ABMC			
Case	N (Visible DRs)	Distance (cm)	N (Not visible DRs)	Distance (cm)	N (Visible DRs)	Distance (cm)	N (Not visible DRs)	Distance (cm)
1	15	1.5± 0.4	10	2.8 ± 0.78	15	0.62± 0.21	10	1.1 ± 0.16
2	15	1.4 ± 0.37	10	2.6 ± 0.4	15	0.87 ± 0.1	10	1.8 ± 0.14
3	20	2.5 ± 0.33	10	3.5 ± 0.45	20	1.4 ± 0.24	10	1.7 ± 0.33
4	23	1.8 ± 0.56	12	2.9 ± 0.62	23	1.1 ± 0.17	12	2.2 ± 0.21
5	20	1.4 ± 0.37	15	2.6 ± 0.4	20	0.75 ± 0.16	15	1.4 ± 0.15

TABLE III: The relative distance between the location of the main identified source for DRs or IEDs and the lead channel at seizure source and the average ASCI number between the IED and DR templates.

Case	DR segments	IED segments	Source distance DR	Source distance IED	Hyperexcitable region	Average ASCI
1	20	30	0.62± 0.21	0.65± 0.18	Posterior and lateral aspects of the left temporal lobe	0.84
2	15	25	0.87 ± 0.1	1.23 ± 0.14	Posterior medial and lateral aspects of the frontal lobe	0.81
3	20	30	1.3 ± 0.24	1.14 ± 0.33	Anterior temporal pole right	0.83
4	23	35	1.1 ± 0.17	1.2 ± 0.11	Tpole and mesiotemporal right	0.80
5	20	25	0.87 ± 0.16	1.24 ± 0.31	Mid-temporal lobe right	0.75

the results. Additionally, the geometry of the subdural mat is limited to the gold-standard clinical assessment equipment available for all the subjects included in the study (standard sizes commonly used in SPES sessions). Due to this limitation, we could not test the ABMC approach with different geometries for the same subject. Typically, the arrangement of the sensor array and the distance between the individual sensors play a crucial role in various aspects, such as spatial resolution, interference suppression, and robustness. Also, reducing the spacing between contacts can generally enhance spatial resolution, allowing the beamformer to separate closely spaced sources more effectively. Also, suitably selected sensor spacing can maximize the array gain by exploiting spatial diversity and constructive interference among array elements. This is a fact worth considering for future research.

VI. Conclusion

In this research, we tried to answer a crucial question raised by epileptologists who apply deep brain stimulation for seizure source identification. The question is whether, for an epileptic patient, the IEDs and DRs to SPES originate from the same location and how accurately this location can be estimated. Here, by developing a suitable beamformer, namely ABMC, we concluded that for our pool of patients and over multiple trials, the sources of these two activities are highly likely to come from the same source in the brain. Clinicians can use this information to manage patients better and plan their treatment more time-efficiently and clinically robustly. In addition, the proposed beamformer's robustness and accuracy have been investigated and compared with those of the conventional approaches, and its superiority has been demonstrated. This is incredibly encouraging for invasive intracranial and high-density non-invasive EEG recordings that need a robust source localization algorithm to aid clinical diagnosis.

References

[1] B. Abdi-Sargezeh, S. Shirani, S. Sanei, C. C. Took, O. Geman, G. Alarcon, and A. Valentin, "A review of signal processing and machine learning techniques for interictal epileptiform discharge detection," *Computers in Biology and Medicine*, p. 107782, 2023.

[2] G. Alarcon, C. Guy, C. Binnie, S. Walker, R. Elwes, and C. Polkey, "Intracerebral propagation of interictal activity in partial epilepsy: implications for source localisation." *Journal of Neurology, Neurosurgery & Psychiatry*, vol. 57, no. 4, pp. 435–449, 1994.

[3] J. F. Torre, G. Alarcon, C. Binnie, and C. Polkey, "Comparison of sphenoidal, foramen ovale and anterior temporal placements for detecting interictal epileptiform discharges in presurgical assessment for temporal lobe epilepsy," *Clinical Neurophysiology*, vol. 110, no. 5, pp. 895–904, 1999.

[4] A. Valentín, G. Alarcón, S. F. Barrington, J. J. G. Seoane, M. C. Martín-Miguel, R. P. Selway, and M. Koutroumanidis, "Interictal estimation of intracranial seizure onset in temporal lobe epilepsy," *Clinical Neurophysiology*, vol. 125, no. 2, pp. 231–238, 2014.

[5] A. Valentin, M. Anderson, G. Alarcon, J. G. Seoane, R. Selway, C. Binnie, and C. Polkey, "Responses to single pulse electrical stimulation identify epileptogenesis in the human brain in vivo," *Brain*, vol. 125, no. 8, pp. 1709–1718, 2002.

[6] A. Valentin, G. Alarcon, J. J. Garcia-Seoane, M. Lacruz, S. Nayak, M. Honavar, R. P. Selway, C. Binnie, and C. Polkey, "Single-pulse electrical stimulation identifies epileptogenic frontal cortex in the human brain," *Neurology*, vol. 65, no. 3, pp. 426–435, 2005.

[7] D. Flanagan, A. Valentín, J. J. García Seoane, G. Alarcón, and S. G. Boyd, "Single-pulse electrical stimulation helps to identify epileptogenic cortex in children," *Epilepsia*, vol. 50, no. 7, pp. 1793–1803, 2009.

[8] R. Matsumoto, T. Kunieda, and D. Nair, "Single pulse electrical stimulation to probe functional and pathological connectivity in epilepsy," *Seizure*, vol. 44, pp. 27–36, 2017.

[9] A. Valentín, G. Alarcón, M. Honavar, J. J. G. Seoane, R. P. Selway, C. E. Polkey, and C. D. Binnie, "Single pulse electrical stimulation for identification of structural abnormalities and prediction of seizure outcome after epilepsy surgery: a prospective study," *The Lancet Neurology*, vol. 4, no. 11, pp. 718–726, 2005.

[10] G. Alarcón, D. Jiménez-Jiménez, A. Valentín, and D. Martín-López, "Characterizing EEG cortical dynamics and connectivity with responses to single pulse electrical stimulation (SPES)," *International Journal of Neural Systems*, vol. 28, no. 06, p. 1750057, 2018.

[11] D. Nayak, A. Valentín, R. P. Selway, and G. Alarcón, "Can single pulse electrical stimulation provoke responses similar to spontaneous interictal epileptiform discharges?" *Clinical Neurophysiology*, vol. 125, no. 7, pp. 1306–1311, 2014.

[12] S. Shirani, A. Valentin, G. Alarcon, F. Kazi, and S. Sanei, "Separating inhibitory and excitatory responses of epileptic brain to single-pulse

electrical stimulation," *International Journal of Neural Systems*, vol. 33, no. 02, p. 2350008, 2023.

[13] ——, "Response to the discussion on s. shirani, a. valentin, g. alarcon, f. kazi and s. sanei, separating inhibitory and excitatory responses of epileptic brain to single-pulse electrical stimulation," *International Journal of Neural Systems*, p. 2375002, 2023.

[14] B. D. Van Veen and K. M. Buckley, "Beamforming: A versatile approach to spatial filtering," *IEEE assp magazine*, vol. 5, no. 2, pp. 4–24, 1988.

[15] J. C. Chen, K. Yao, and R. E. Hudson, "Source localization and beamforming," *IEEE Signal Processing Magazine*, vol. 19, no. 2, pp. 30–39, 2002.

[16] L. S. Resende, J. M. T. Romano, and M. G. Bellanger, "A fast least-squares algorithm for linearly constrained adaptive filtering," *IEEE Transactions on Signal Processing*, vol. 44, no. 5, pp. 1168–1174, 1996.

[17] B. D. Van Veen, W. Van Drongelen, M. Yuchtman, and A. Suzuki, "Localization of brain electrical activity via linearly constrained minimum variance spatial filtering," *IEEE Transactions on Biomedical Engineering*, vol. 44, no. 9, pp. 867–880, 1997.

[18] X. Guo, L. Chu, and B. Li, "Robust adaptive LCMV beamformer based on an iterative suboptimal solution," *Radioengineering*, vol. 24, no. 2, pp. 572–582, 2015.

[19] S. Shirani, A. Valentin, B. Abdi-Sargezeh, G. Alarcon, and S. Sanei, "Localization of epileptic brain responses to single-pulse electrical stimulation by developing an adaptive iterative linearly constrained minimum variance beamformer." *International Journal of Neural Systems*, pp. 2 350 050–2 350 050, 2023.

[20] C. Cai, Y. Long, S. Ghosh, A. Hashemi, Y. Gao, M. Diwakar, S. Haufe, K. Sekihara, W. Wu, and S. S. Nagarajan, "Bayesian adaptive beamformer for robust electromagnetic brain imaging of correlated sources in high spatial resolution," *IEEE Transactions on Medical Imaging*, 2023.

[21] S. Sanei and J. A. Chambers, *EEG signal processing and machine learning*. John Wiley & Sons, 2021.

[22] J. Engel Jr, "Surgery for seizures," *New England Journal of Medicine*, vol. 334, no. 10, pp. 647–653, 1996.

[23] V. Kokkinos, G. Alarcón, R. P. Selway, and A. Valentín, "Role of single pulse electrical stimulation (SPES) to guide electrode implantation under general anaesthesia in presurgical assessment of epilepsy," *Seizure*, vol. 22, no. 3, pp. 198–204, 2013.

[24] T. Babb, W. Brown, and J. J. Engel, "Surgical treatment of the epilepsies," *New York, NY*, 1987.

[25] A. Horn and A. A. Kühn, "Lead-DBS: a toolbox for deep brain stimulation electrode localizations and visualizations," *Neuroimage*, vol. 107, pp. 127–135, 2015.

[26] S. Ewert, A. Horn, F. Finkel, N. Li, A. A. Kühn, and T. M. Herrington, "Optimization and comparative evaluation of nonlinear deformation algorithms for atlas-based segmentation of dbs target nuclei," *Neuroimage*, vol. 184, pp. 586–598, 2019.

[27] B. B. Avants, C. L. Epstein, M. Grossman, and J. C. Gee, "Symmetric diffeomorphic image registration with cross-correlation: evaluating automated labeling of elderly and neurodegenerative brain," *Medical Image Analysis*, vol. 12, no. 1, pp. 26–41, 2008.

[28] T. Schönecker, A. Kupsch, A. Kühn, G.-H. Schneider, and K.-T. Hoffmann, "Automated optimization of subcortical cerebral MR imaging-atlas coregistration for improved postoperative electrode localization in deep brain stimulation," *American Journal of Neuroradiology*, vol. 30, no. 10, pp. 1914–1921, 2009.

[29] R. Oostenveld, P. Fries, E. Maris, and J.-M. Schoffelen, "Fieldtrip: open source software for advanced analysis of MEG, EEG, and invasive electrophysiological data," *Computational Intelligence and Neuroscience*, vol. 2011, pp. 1–9, 2011.

[30] T. S. Davis, R. M. Caston, B. Philip, C. M. Charlebois, D. N. Anderson, K. E. Weaver, E. H. Smith, and J. D. Rolston, "Legui: a fast and accurate graphical user interface for automated detection and anatomical localization of intracranial electrodes," *Frontiers in Neuroscience*, vol. 15, p. 769872, 2021.

[31] M. I. Jordan, Z. Ghahramani, T. S. Jaakkola, and L. K. Saul, "An introduction to variational methods for graphical models," *Machine Learning*, vol. 37, pp. 183–233, 1999.

[32] C. Cai, A. Hashemi, M. Diwakar, S. Haufe, K. Sekihara, and S. S. Nagarajan, "Robust estimation of noise for electromagnetic brain imaging with the champagne algorithm," *NeuroImage*, vol. 225, p. 117411, 2021.

[33] D. Wipf and S. Nagarajan, "A unified bayesian framework for MEG/EEG source imaging," *NeuroImage*, vol. 44, no. 3, pp. 947–966, 2009.

[34] K. Sekihara and S. S. Nagarajan, *Electromagnetic brain imaging: A Bayesian perspective*. Springer, 2015.

[35] J. Lian, G. Garner, D. Muessig, and V. Lang, "A simple method to quantify the morphological similarity between signals," *Signal Processing*, vol. 90, no. 2, pp. 684–688, 2010.

[36] P. Chauhan, S. E. Philip, G. Chauhan, and S. Mehra, "The anatomical basis of seizures," *Epilepsy [Internet]*, 2022.

[37] L. G. Dominguez, A. Tarazi, T. Valiante, and R. Wennberg, "Beamforming seizures from the temporal lobe using magnetoencephalography," *Canadian Journal of Neurological Sciences*, vol. 50, no. 2, pp. 201–213, 2023.

[38] S. Parmigiani, E. Mikulan, S. Russo, S. Sarasso, F. Zauli, A. Rubino, A. Cattani, M. Fecchio, D. Giampiccolo, J. Lanzone *et al.*, "Simultaneous stereo-EEG and high-density scalp EEG recordings to study the effects of intracerebral stimulation parameters," *Brain Stimulation*, vol. 15, no. 3, pp. 664–675, 2022.